RESEARCH ARTICLE

The static and free vibration analyses of axially functionally graded elliptical beams via mixed FEM

Merve Ermis[1], Gokay Aydogan[1], Oguzhan Kir[1], Umit N. Aribas[2],

Mehmet H. Omurtag [2]

[1] Kirklareli University, Department of Civil Engineering, Kirklareli, Türkiye
[2] Istanbul Medipol University, Department of Civil Engineering, Istanbul, Türkiye

Abstract

The objective of this study is to investigate the behavior of the static and free vibration analyses of axially functionally graded elliptical planar curved beams using a mixed finite element method (MFEM) based on the Timoshenko beam theory. A two-noded curved mixed finite element has 12 field variables at each node. These variables denote three displacements, three cross-sectional rotations, three forces, two bending moments, and torque, respectively. The functionally graded material is composed of ceramic-particle material and metal-matrix material. The volume fraction of ceramic and metal materials varies along the beam axis. The effective material properties (modulus of elasticity, Poisson's ratio, and density) of the functionally graded material are determined according to the rule of mixture. It is aimed in the benchmark examples to present the influence of ceramic-particle material and non-homogeneity index of material gradation, the minimum radius of the elliptical beam, and boundary condition to the results of static and free vibration analysis in detail.

1. Introduction

Functionally graded materials are a new generation of composite materials that are widely used in aerospace, energy, automotive, defense, and nuclear industries, civil engineering, as well as in optical, electronic, and biomedical devices or chemical plants [1-11]. Due to abrupt changes in thermal conditions or mechanical loads, problems of cracks or delamination can occur in structures having classical composite material properties (e.g. laminated composites). Functionally graded (FG) materials are two-phase composite materials with a continuously varying function in desired directions. The grading of material properties increases the strength of functionally graded materials under sudden varying loads or temperature changes [12,13]. Functionally graded materials are produced with low thermal conductivity, high hardness and wear resistance, and other excellent mechanical and chemical properties such as low coefficient of friction [14].

Curved beams are commonly used structural elements in architecture, and civil and mechanical engineering applications e.g. [15-18]. In the literature, most studies about the structural analysis of axially FG beams are related to straight beam geometry. Some of the studies can be cited as follows [19-31] for the static/buckling/dynamic analysis of axially FG straight beams/micro or nanobeams. Some studies about the structural analysis of axially functional graded (AFG) curved planar beams can be summarized as follows:

Rajesakaran [32] investigated the static and free vibration analyses of AFG curved beams using the differential transformation method in which the shear effect was considered. Tsiatas and Charalampakis [33] dealt with the optimization problem over the natural frequencies of AFG straight and circular planar beams with material distribution described by a four-parameter exponential function or a five-parameter trigonometric function. Noori et. al. [34] investigated the free vibration and forced vibration analyses of AFG parabolic beams using the complementary functions method. Temel and Noori [35] investigated the free vibration and forced vibration analyses of AFG cycloid beams with variable cross-sections using the complementary functions method by considering the shear effects of the beam. Lee and Lee [36] investigated the free vibration behavior of AFG circular beams using the direct integral method developed with the trial eigenvalue method. Arıbas et.al. [37] investigated the static response and normal/shear stresses of AFG exact super-elliptical beams via a warping-included mixed finite element method. Aktı et.al.[38] investigated the behavior of the static analysis of AFG circular planar curved beams using a mixed finite element method (MFEM) based on Timoshenko beam theory. Convergence analysis of AFG elliptical beams is investigated over 3-D 2 node beam element (BEAM188) and 3-D 20-Node structural solid element (SOLID186) of ANSYS finite element program for the static and free vibration analysis by Kır et.al. [39] and Aydoğan et. al. [40], respectively.

In this study, the static and free vibration of axially FG elliptical curved beams are investigated using mixed FEM. The FG material is composed of a metal matrix reinforced with ceramic-particle material. In the static analysis, the influence of ceramic material (Al_2O_3, ZrO_2, and SiC), boundary conditions (fixed-fixed and fixed free), and non-homogeneity index of material gradation on the response of axially FG elliptical beam subjected to a vertical uniformly distributed load are investigated over the displacement, cross-sectional rotations, and support reactions of the beam in detail. In the free vibration analysis, the out-of-plane natural frequencies are examined for the same parameters as those considered in the static analysis. As far as the authors know, this study is a new contribution to the literature and provides some benchmark examples.

2. Formulation

2.1. Elliptical beam geometry

A planar curve is described by a position vector r(θ) in an *x-y* plane in terms of a horizontal angle θ as follows:

$$\mathbf{r}(\theta) = \{x(\theta), y(\theta)\} \tag{1}$$

For an elliptical beam (Fig. 1), the components in the *x-y* plane of the position vector *x-y*, are

$$x(\theta) = R_{\max} \cos \theta, \quad y(\theta) = R_{\min} \sin \theta \tag{2}$$

where $R_{\min} > 0$ and $R_{\max} > 0$ are the minimum and maximum radii, respectively. The gradient of the arc length $c(\theta)$ is defined in terms of the position vector Eq. (1) as follows:

$$c(\theta) = \left\| \mathbf{r}_{,\theta} \right\|, \quad \mathrm{d}s = c(\theta)\,\mathrm{d}\theta \tag{3}$$

where the subscript after the comma denotes a derivative with respect to horizontal angle θ [41], ds is the infinitesimal arc length. The total length S of the elliptical beam is calculated using $S = \int_0^{\theta_B} c(\theta)\,\mathrm{d}\theta$ where θ_B is the subtended angle of the elliptical beam.
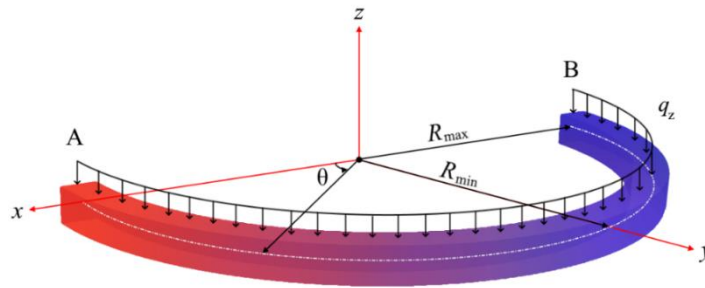
Fig. 1. Axially functionally graded elliptical beam

Table 1. The material properties of ceramic particles and metal matrix.

Material	E (GPa)	v	ρ (kg/m^3)
Aluminum (Al) [44]	70	0.3	2702
Alumina (Al$_2$O$_3$) [44]	380	0.3	3800
Zirconia (ZrO$_2$) [44]	200	0.3	5700
Silicon carbide (SiC) [45]	302	0.17	3200

2.2. Axially functionally graded material

A two-phase composite beam is composed of a metal matrix and ceramic particles. The variation of the material along the beam axis depends on the horizontal angle θ (Fig.1). As a homogenization scheme, the Voigt model [42,43] is used to predict the effective material properties of a two-phase composite beam as follows:

$$P_{\text{eff}}\left(\theta\right) = P_{\text{A}} + \left(P_{\text{B}} - P_{\text{A}}\right)\left(\frac{\theta}{\theta_B}\right)^{n_h} \tag{4}$$

where P_{eff} denotes the effective material properties of the modulus of elasticity (E), Poisson's ratio (v), and density (ρ), respectively. $n_h \geq 0$ is the non-homogeneity index of material gradation. The subscripts A and B denote the metal and ceramic materials at the start and endpoints of the elliptical beam, respectively. In this study, three different ceramic materials (Al$_2$O$_3$, ZrO$_2$, SiC) are employed while the metal matrix (Al) is kept the same. The material properties are given in Table 1.

The variation of the material constituents along the beam axis can be determined using Eq. (4) and the material properties in Table 1. The material variation versus normalized horizontal angle parameter (θ/θ_B) is plotted for different non-homogeneity indices and three different ceramic materials (Al$_2$O$_3$, SiC, and ZrO$_2$) in Fig.2

2.3. Field equations, functional and mixed finite element formulation

The field equations in the Frenet coordinate system of axially curved beams are extended from the isotropic spatial Timoshenko beam [46] as

$$\left.\begin{array}{r} -\mathbf{T}_{,s} - \mathbf{q} + \rho A \ddot{\mathbf{u}} = \mathbf{0} \\ -\mathbf{M}_{,s} - \mathbf{t} \times \mathbf{T} - \mathbf{m} + \rho \mathbf{I} \ddot{\mathbf{\Omega}} = \mathbf{0} \end{array}\right\} \quad \text{equations of motion} \tag{5}$$
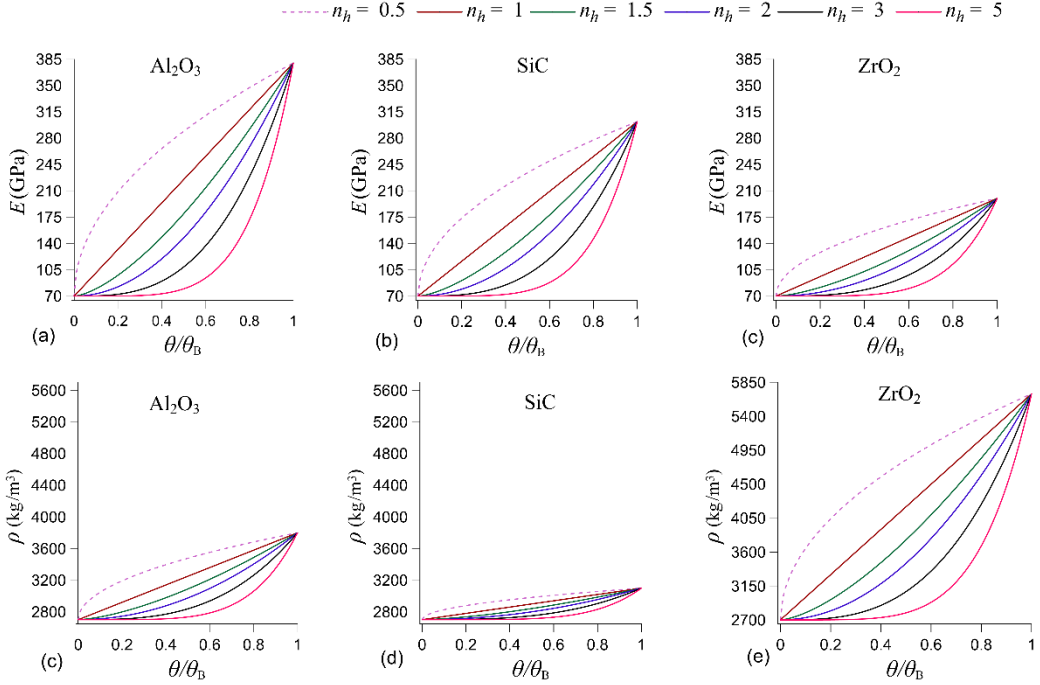
Fig. 2. The effective material properties of axially functionally graded material composed of metal-matrix (Al) reinforced by three different ceramic particles (Al₂O₃, SiC, and ZrO₂)

$$\left.\begin{array}{c} \mathbf{u}_{,s} + \mathbf{t} \times \mathbf{\Omega} - \mathbf{C}_{\gamma}\,\mathbf{T} = \mathbf{0} \\[4pt] \mathbf{\Omega}_{,s} - \mathbf{C}_{\kappa}\,\mathbf{M} = \mathbf{0} \end{array}\right\} \quad \text{constitutive equations} \tag{6}$$

where t, n and b are the tangent, normal and binormal unit vectors of Frenet coordinate. $\mathbf{u}(u_t, u_n, u_b)$ is the displacement vector, $\mathbf{\Omega}(\Omega_t, \Omega_n, \Omega_b)$ is the cross-sectional rotation vector, $\mathbf{T}(T_t, T_n, T_b)$ is the force vector and $\mathbf{M}(M_t, M_n, M_b)$ is the moment vector, $\mathbf{q}(q_t, q_n, q_b)$ is the distributed load, $\mathbf{m}(m_t, m_n, m_b)$ is the distributed moment, $\rho = \rho(\theta)$ is the material density of the axially FG beam, A is the cross-sectional area, $\mathbf{I}(I_t, I_n, I_b)$ is the moment of inertia vector, $\mathbf{C}_{\gamma} = \mathbf{C}_{\gamma}(\theta)$ and $\mathbf{C}_{\kappa} = \mathbf{C}_{\kappa}(\theta)$ are the compliance matrices of the axially FG beam.

The functional for free vibration and static analyses of the isotropic homogenous elastic spatial beam exists in [46,47]. The functional for free vibration analysis of the axially functionally graded spatial beam is given in Ermis 2021 [48]. Using the potential operator and Gâteaux differential [49], the functional [46] in terms of Eq. (5) and (6) yields to the necessary form for static analysis of the AFG spatial beam can be given as follows:

$$\left.\begin{array}{l} \mathbf{I}(\mathbf{y}) = -\big[\mathbf{u}, \mathbf{T}_{,s}\big] + \big[\mathbf{t} \times \mathbf{\Omega}, \mathbf{T}\big] - \big[\mathbf{M}_{,s}, \mathbf{\Omega}\big] - \dfrac{1}{2}\big[\mathbf{C}_{\kappa}(\theta)\mathbf{M}, \mathbf{M}\big] - \dfrac{1}{2}\big[\mathbf{C}_{\gamma}(\theta)\mathbf{T}, \mathbf{T}\big] \\[8pt] \quad -\big[\mathbf{q}, \mathbf{u}\big] - \big[\mathbf{m}, \mathbf{\Omega}\big] + \big[(\mathbf{T} - \hat{\mathbf{T}}), \mathbf{u}\big]_{\sigma} + \big[(\mathbf{M} - \hat{\mathbf{M}}), \mathbf{\Omega}\big]_{\sigma} + \big[\hat{\mathbf{u}}, \mathbf{T}\big]_{\varepsilon} + \big[\mathbf{\Omega}, \mathbf{M}\big]_{\varepsilon} \end{array}\right\} \tag{7}$$

Considering the harmonic motion in the free vibration analysis, Eq. (7) can be rearranged by using $\mathbf{q} = \mathbf{m} = 0$ and inserting the acceleration terms in the form $\frac{1}{2}\rho(\theta)[\ddot{\mathbf{u}}, \ddot{\mathbf{u}}] = -\frac{1}{2}\rho(\theta)\omega^2[\mathbf{u}, \mathbf{u}]$, $\frac{1}{2}\rho(\theta)[\ddot{\mathbf{\Omega}}, \ddot{\mathbf{\Omega}}] = -\frac{1}{2}\rho(\theta)\omega^2[\mathbf{\Omega}, \mathbf{\Omega}]$ where ω is the natural circular frequency. The parentheses in Eq. (7) indicate the inner product, the terms with hats are known values on the boundary and the subscripts ε and σ

represent the geometric and dynamic boundary conditions, respectively. It is noted that the unit vector b coincides with the unit vector z for a planar beam defined in the x-y plane.

For the finite element formulation, the linear shape functions $\Phi_i = (\varphi_j-\varphi)/\Delta\varphi$ and $\Phi_j = (\varphi-\varphi_i)/\Delta\varphi$ are employed in finite element formulation. The subscripts represent the node number of the curved finite element, $\varphi_j > \varphi_i$ and $\Delta\varphi =(\varphi_j- \varphi_i)$. The mixed type curved finite element has two nodes with 2×12 degrees of freedom as follows: three displacements, three cross-sectional rotations, a normal force, two shear forces, two bending moments, and a torque. The detailed information for the submatrices of the mixed-type finite element matrix exists in [46].

3. Numerical examples

This section aims to investigate the effect of different ceramic particle materials, the non-homogeneity index (n_h), minimum radius (R_{min}), and boundary conditions on the static and dynamic responses of the AFG elliptical beam. Firstly, the convergence and comparison problems are handled between MFEM and ANSYS [50] for static and free vibration analyses in Sec.3.1. Next, some benchmark examples are introduced to the literature in Sec.3.2. Throughout the numerical examples, the common geometric parameters are as follows: the maximum radius $R_{max} = 10$m and the subtended angle $\theta_B = 180°$ of the elliptical beam. The width and height of the rectangular cross-section is 0.48 m and 0.36 m, respectively. For the static analysis, the vertical distributed load is $q(z) = 1$ N/m.
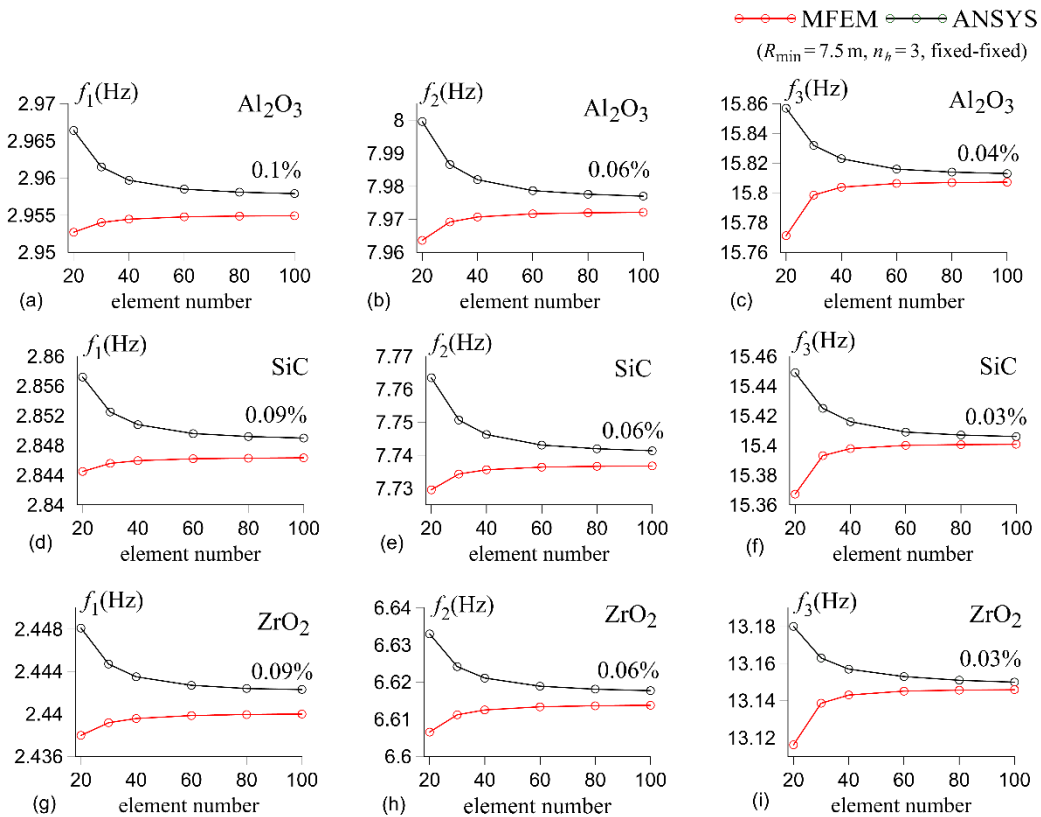

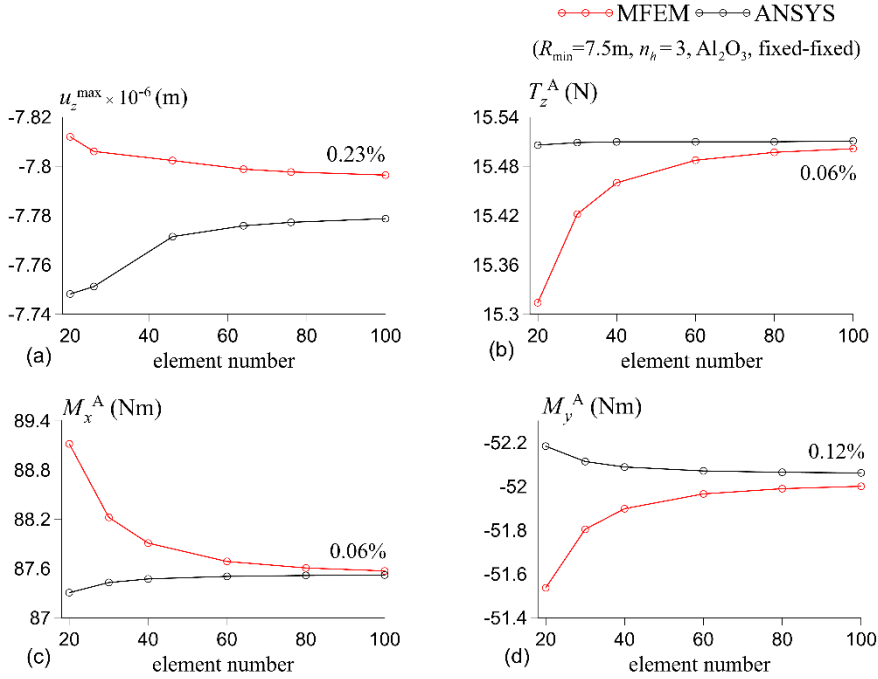Fig. 3. The convergence analysis for natural frequencies of AFG elliptical beams

Fig.4. The convergence analysis for the static response of the AFG elliptical beam (Al- Al_2O_3) having fixed-fixed BC

3.1. Convergence and comparison study

In this section, convergency analysis and comparison between MFEM and ANSYS-BEAM188 are carried out for the free vibration (Sec.3.1.1.) and static analysis (Sec.3.1.2.) of AFG elliptical beams. The minimum radius is considered as R_{min} = 7.5 m, the non-homogeneity index is n_h = 3 and the boundary condition is fixed at both ends of the beam. In ANSYS analysis, the BEAM188 element, two noded beam elements in 3D, is used. BEAM188 has six degrees of freedom at each node. Three of them are translations along x, y, and z-directions. The remaining ones are rotations about x, y, and z-directions.

3.1.1. Free vibration analysis

Three different ceramic particles are considered as: Al_2O_3, ZrO_2, and SiC. The convergence analysis MFEM and ANSYS for the first three out-of-plane natural frequencies of the AFG elliptical beam is plotted against the number of elements between n_e = 20 and 100 in Fig.3. The percent differences of the results are calculated using $\text{diff.}\% = \left(1 - f_1^{\text{MFEM}} / f_1^{\text{ANSYS}}\right) \times 100$ and are given in Fig. 3 for n_e = 100 finite elements. The maximum percent difference is 0.1%. The convergence rate of the first natural frequency of AFG elliptical beams calculated by MFEM is considerably faster than the results obtained by ANSYS-BEAM188 for all the considered ceramic-particle materials.

3.1.2. Static analysis

Al_2O_3 ceramic material is employed. The convergence analysis MFEM and ANSYS for the static responses (u_z^{max} , T_z^A , M_x^A , and M_y^A) of the AFG elliptical beam is plotted against the number of elements between n_e = 20 and 100 in Fig. 4. It is noted that the maximum displacement u_z^{max} occurs at 0.432 which is the normalized arc length of the AFG beam for n_e = 100. The results obtained by MFEM are compared to those of ANSYS, and the percent differences for n_e = 100 finite elements are given in Fig. 4 for each static response

($u_z^{\max}$, T_z^{A} , M_x^{A} , and M_y^{A}). The maximum percent difference is 0.23%. It can be said that the convergence rate of the maximum displacement $u_z^{\max}$ of AFG elliptical beams calculated by MFEM is faster than the results obtained by ANSYS-BEAM188 whereas the convergence rate of the static response (T_z^{A} , M_x^{A} , and M_y^{A}) of AFG elliptical beams calculated by ANSYS-BEAM188 is significantly faster than MFEM.

For both free vibration and static analyses, it is observed that the results of MFEM and ANSYS are consistent with each other in Sec. 3.1.1 and 3.1.2, respectively. n_e =100 finite elements provide enough precision results for the dynamic response (the first three out-of-plane natural frequencies) and static responses ($u_z^{\max}$, T_z^{A} , M_x^{A} , and M_y^{A}) of the AFG elliptical beam. In the following benchmark examples, the results of static and free vibration analyses, n_e =100 is used.

Table 2. The fundamental natural frequencies f (in Hz) of the AFG elliptical planar beam. (Al-Al₂O₃)

Boundary conditions	$R_{\min}$ (m)	The non-homogeneity index (n_h)					
		0.5	1	1.5	2	3	5
fixed-free	5	0.734	0.605	0.547	0.519	0.496	0.489
	7.5	0.584	0.481	0.436	0.415	0.398	0.394
	10	0.477	0.393	0.357	0.340	0.326	0.323
fixed-fixed	5	4.941	4.558	4.360	4.226	4.039	3.808
	7.5	3.477	3.230	3.122	3.054	2.955	2.814
	10	2.488	2.326	2.265	2.230	2.176	2.085

Table 3. The fundamental natural frequencies f (in Hz) of the AFG elliptical planar beam. (Al-SiC)

Boundary conditions	$R_{\min}$ (m)	The non-homogeneity index (n_h)					
		0.5	1	1.5	2	3	5
fixed-free	5	0.746	0.626	0.571	0.543	0.520	0.509
	7.5	0.597	0.500	0.457	0.436	0.419	0.411
	10	0.489	0.409	0.375	0.358	0.344	0.338
fixed-fixed	5	4.867	4.459	4.240	4.095	3.902	3.685
	7.5	3.428	3.162	3.036	2.955	2.846	2.711
	10	2.454	2.276	2.200	2.153	2.089	2.000

Table 4. The fundamental natural frequencies f (in Hz) of the AFG elliptical planar beam. (Al-ZrO₂)

Boundary conditions	$R_{\min}$ (m)	The non-homogeneity index (n_h)					
		0.5	1	1.5	2	3	5
fixed-free	5	0.490	0.446	0.429	0.423	0.425	0.439
	7.5	0.392	0.356	0.343	0.338	0.339	0.350
	10	0.321	0.291	0.280	0.277	0.277	0.286
fixed-fixed	5	3.254	3.245	3.281	3.319	3.364	3.371
	7.5	2.305	2.311	2.352	2.391	2.440	2.457
	10	1.655	1.666	1.703	1.737	1.780	1.798

3.2. Benchmark examples

Throughout the analysis, the following parameters are used: the minimum radius is $R_{min} = 5$ m, 7.5 m, and 10 m. The metal matrix (Al) is reinforced by three different ceramic particle materials Al_2O_3, ZrO_2, and SiC, respectively. The non-homogeneity index of the functionally graded material is $n_h = 0.5, 1, 1.5, 2, 3$ and 5, respectively. The boundary conditions are fixed-fixed and fixed-free, respectively.

3.2.1. Free vibration analysis

The fundamental natural frequencies f of AFG beam are tabulated in Tables 2-4 for the minimum radius $R_{min} = 5$ m, 7.5 m, and 10 m, respectively. By considering the results for all of the considered minimum radii cases (Tables 2-4): In the case of fixed-free BC, when the non-homogeneity index (n_h) increases, the fundamental natural frequencies decrease for all the considered ceramic-particle cases. In the case of fixed-fixed BC, when the non-homogeneity index (n_h) increases, the fundamental natural frequencies decrease for Al_2O_3 and SiC whereas the fundamental natural frequencies increase for ZrO_2. The conclusions of parametric studies are handled in the following three sub-sections in detail.

3.2.1.1. The effect of the non-homogeneity index (n_h)

To investigate the effect of the non-homogeneity index on the fundamental natural frequencies (f) of AFG elliptical beam, the results of the cases $n_h = 1, 1.5, 2, 3,$ and 5 are compared with the results of the case $n_h = 0.5$ by using $\beta_{n_h=i} = f_{n_h=i}/f_{n_h=0.5}$ where ($i = 1, 1.5, 2, 3,$ and 5) for each boundary condition, minimum radius, and ceramic material. For the fixed-fixed boundary condition, the ratio $\beta_{n_h=i}$ is plotted against $R_{min} = 5$ m, 7.5 m, and 10 m in Fig.5a, b, and c for the ceramic materials Al_2O_3, SiC, and ZrO_2, respectively. It should be noted that when the non-homogeneity index (n_h) decreases, the constituent of functionally graded material along the beam axis becomes ceramic-rich material (Fig. 2a-c). On the other hand, when the non-homogeneity index (n_h) increases, the constituent of functionally graded material along the beam axis becomes metal-rich material (Fig. 2a-c). The following outcomes can be stated for each value R_{min} over the β_{n_h}:

1. For the fixed-fixed boundary condition, the maximum fundamental natural frequencies of the cases Al_2O_3 and SiC (see Fig. 5a and b) are obtained for the $n_h = 0.5$, and the values of β_{n_h} are less than 1. Also, when the non-homogeneity index (n_h) increase, the ratio β_{n_h} decreases.
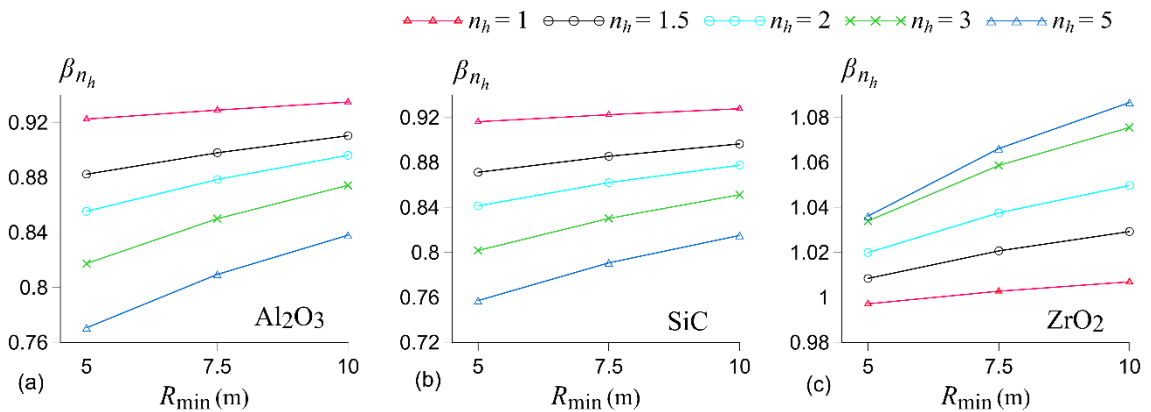

Fig. 5. The effect of the non-homogeneity index on the fundamental natural frequencies of AFG elliptical beam having fixed-fixed BC, $\beta_{n_h=i} = f_{n_h=i}/f_{n_h=0.5}$ where ($i = 1, 1.5, 2, 3,$ and 5).

2. The maximum fundamental natural frequencies for ZrO_2 (see Fig. 5c) are obtained for the $n_h = 5$. When the non-homogeneity index (n_h) decreases, the ratio β_{n_h} decreases.

3. As the ratio β_{n_h} becomes closer to 1, the fundamental natural frequencies of the non-homogeneity indices approach the results of $n_h = 0.5$. It means when $\beta_{n_h} \rightarrow 1$, the effect of the constituent ceramic-rich or metal-rich functionally graded material on the fundamental natural frequency results of AFG beams is less influential for the case ZrO_2 (e.g. the cases $R_{min} = 5$ m and in Fig. 5c). The effect of the constituent ceramic-rich or metal-rich functionally graded material on the fundamental natural frequency results of AFG elliptical beam is more influential for the cases Al_2O_3 and SiC (e.g. the cases $R_{min} = 5$ m and in Fig. 5a and b).

For the fixed-free boundary condition, the maximum fundamental natural frequencies of all the considered ceramic particles and minimum radius R_{min} value are obtained for the $n_h = 0.5$. It is also observed that the ratio $\beta_{n_h = i}$ has nearly the same values for each value of minimum radius. For the selected minimum radius $R_{min} = 5$ m, $\beta_{n_h = i} = 0.825, 0.746, 0.707, 0.676$, and 0.667 for Al_2O_3; $\beta_{n_h = i} = 0.838, 0.765, 0.728, 0.696$, and 0.683 for SiC; $\beta_{n_h = i} = 0.909, 0.875, 0.863, 0.866$ and 0.896 for ZrO_2.

3.2.1.2. The effect of the material properties of ceramic material

To investigate the effect of the ceramic material on the fundamental natural frequencies (f) of AFG elliptical beam, the results of the cases SiC and ZrO_2 are compared with the results of the case Al_2O_3 using $\beta_c = f_c / f_{Al_2O_3}$ where (c = SiC and ZrO_2) for each boundary condition, minimum radius, and the non-homogeneity index. For the minimum radius $R_{min} = 5$ m and both boundary conditions, the ratio β_c is plotted against $n_h = 0.5, 1, 1.5, 2, 3$, and 5 in Fig.6 a and b for the ceramic materials SiC and ZrO_2, respectively.

In the case of SiC (Fig. 6a), the ratio $\beta_{SiC} < 1$ of the fixed-fixed boundary condition is less than 1 for all considered non-homogeneity indexes. It means the maximum fundamental natural frequencies of the fixed-fixed BC case are obtained for ceramic material Al_2O_3. On the other hand, the ratio $\beta_{SiC} > 1$ of the fixed-free boundary condition is greater than 1 for all considered non-homogeneity indexes. It means the maximum fundamental natural frequencies of the fixed-free BC are obtained for ceramic material SiC.
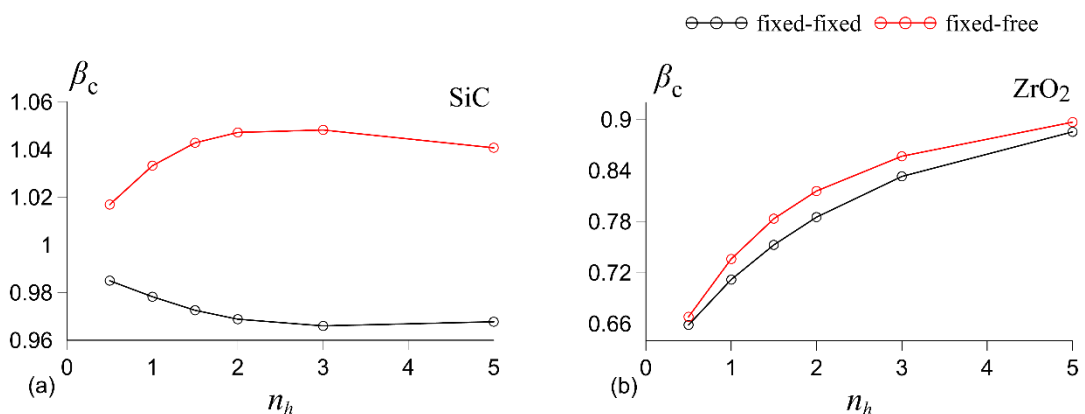

Fig. 6. The effect of ceramic particles on the fundamental natural frequencies of AFG elliptical beam with $R_{min} = 5$ m. $\beta_c = f_c / f_{Al_2O_3}$ (where c: SiC and ZrO_2).
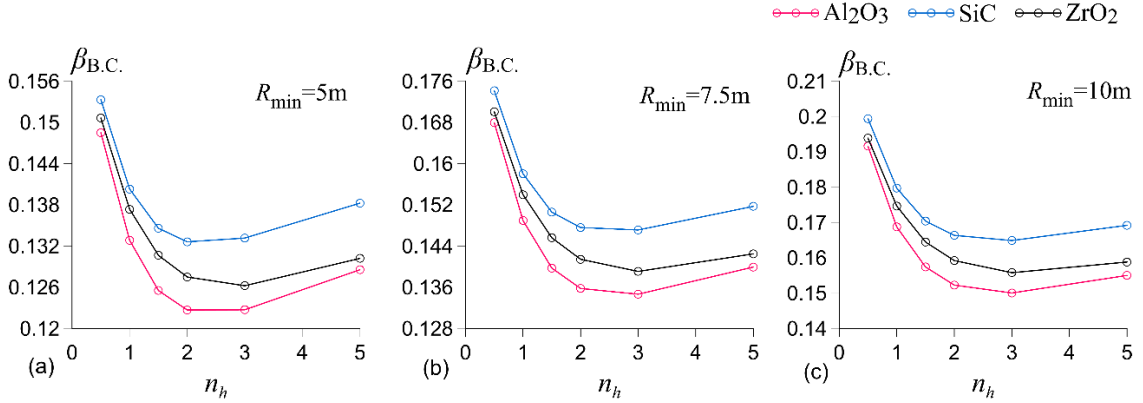
Fig. 7. The effect of boundary conditions on the fundamental natural frequencies of AFG elliptical beam
$$(\beta_{\text{B.C.}} = f_{\text{fixed-free}} / f_{\text{fixed-fixed}})$$

In the case of ZrO_2 case (Fig. 6b), the ratio $\beta_{ZrO_2} < 1$ of fixed-fixed and fixed-free boundary conditions is less than 1 for all considered non-homogeneity indexes. It means the maximum fundamental natural frequencies of the fixed-fixed BC are obtained for ceramic material Al_2O_3.

When the non-homogeneity index increases, the ratio β_{ZrO_2} increases for both boundary conditions. It means the fundamental natural frequencies results of ZrO_2 case approach the results of Al_2O_3 case.

For both boundary conditions, the cases $R_{\text{min}} = 7.5$ m and $R_{\text{min}} = 10$ m show a similar trend to the case $R_{\text{min}} = 5$ m in Fig.6.

As the ratio β_c becomes closer to 1, the fundamental natural frequencies of cases SiC and ZrO_2 approach the results of Al_2O_3. It means the effect of the type of the constituent ceramic material of functionally graded material on the fundamental natural frequency results of AFG elliptical beam is less influential for the case SiC (e.g. the case $n_h = 0.5$ in Fig. 6a).

3.2.1.3. The effect of the boundary condition

To investigate the effect of the boundary conditions on the fundamental natural frequencies (f) of AFG elliptical beam, the results of the fixed-fixed boundary condition are compared with those of the fixed-free one by using $\beta_{\text{B.C.}} = f_{\text{fixed-free}} / f_{\text{fixed-fixed}}$ for each minimum radius and the non-homogeneity index in Fig.7. By considering each ceramic particle, the minimum ratio $\beta_{\text{B.C.}}$ occurs at the case Al_2O_3 for all considered minimum radii and the non-homogeneity indexes.

By considering each case, $e.g.$, the non-homogeneity index and ceramic-particle materials, the minimum ratio $\beta_{\text{B.C.}}$ occurs at $R_{\text{min}} = 5$ m. Also, by considering each case, $e.g.$, ceramic-particle materials, the maximum ratio $\beta_{\text{B.C.}}$ occurs at the case $n_h = 0.5$.

3.2.2. Static analysis

The static responses (u_z^{max}, Ω_x^{max}, Ω_y^{max}, T_z^{A}, M^{A}, and M^{B}) of AFG beam having fixed-fixed BC and minimum radius $R_{\text{min}} = 10$ m are plotted against the non-homogeneity index in Fig. 8. M^{A} and M^{B} are the resultant of the moments at points A and B, respectively (Fig.1).

The normalized arc length coordinates for the maximum displacement $u_z^{\max}$ of AFG planar curved beam with $R_{\max} = 10$ m for the fixed-fixed case are given in Table 5. The static responses ($u_z^{\max}$, $\Omega_x^{\max}$, $\Omega_y^{\max}$) of an AFG beam with a fixed-free BC are plotted versus the non-homogeneity index in Fig. 9. For fixed-free BC, the static responses of T_z^{A} and M^{A} are the same values for all of the considered non-homogeneity indices and ceramic particles. T_z^{A} and M^{A} are found to be -24.221 N and 256.89 Nm for $R_{\min} = 5$ m, -27.629 N and 308.94 Nm for $R_{\min} = 7.5$ m, and -31.415 N and 372.42 Nm for $R_{\min} = 10$ m, respectively.

As the non-homogeneity index decreases, the constituent of functionally graded material along the beam axis becomes ceramic-rich material (Fig.2a-c). Each ceramic particle has both higher elasticity modulus than that of the metal matrix (Al). Thus, the absolute minimum value of $u_z^{\max}$, $\Omega_x^{\max}$, $\Omega_y^{\max}$ occurs at non-homogeneity index $n_h = 0.5$ whereas the absolute maximum value of $u_z^{\max}$, $\Omega_x^{\max}$, $\Omega_y^{\max}$ occurs at non-homogeneity index $n_h = 5$. Also, the ratio Γ of elasticity modulus between ceramic and metal material is calculated using $\Gamma_c^{E} = \Gamma_c^{E} / \Gamma_{Al}^{E}$ where c: Al₂O₃, SiC, and ZrO₂ as follows: $\Gamma_{Al_2O_3}^{E} = 5.43$, $\Gamma_{SiC}^{E} = 4.31$, $\Gamma_{ZrO_2}^{E} = 2.86$, respectively. As the ratio of elasticity modulus Γ increases, the absolute values $u_z^{\max}$, $\Omega_x^{\max}$, $\Omega_y^{\max}$ decrease. The absolute minimum value of $u_z^{\max}$, $\Omega_x^{\max}$, $\Omega_y^{\max}$ is obtained for the Al₂O₃ case whereas the absolute maximum value of $u_z^{\max}$, $\Omega_x^{\max}$, $\Omega_y^{\max}$ is obtained for ZrO₂.
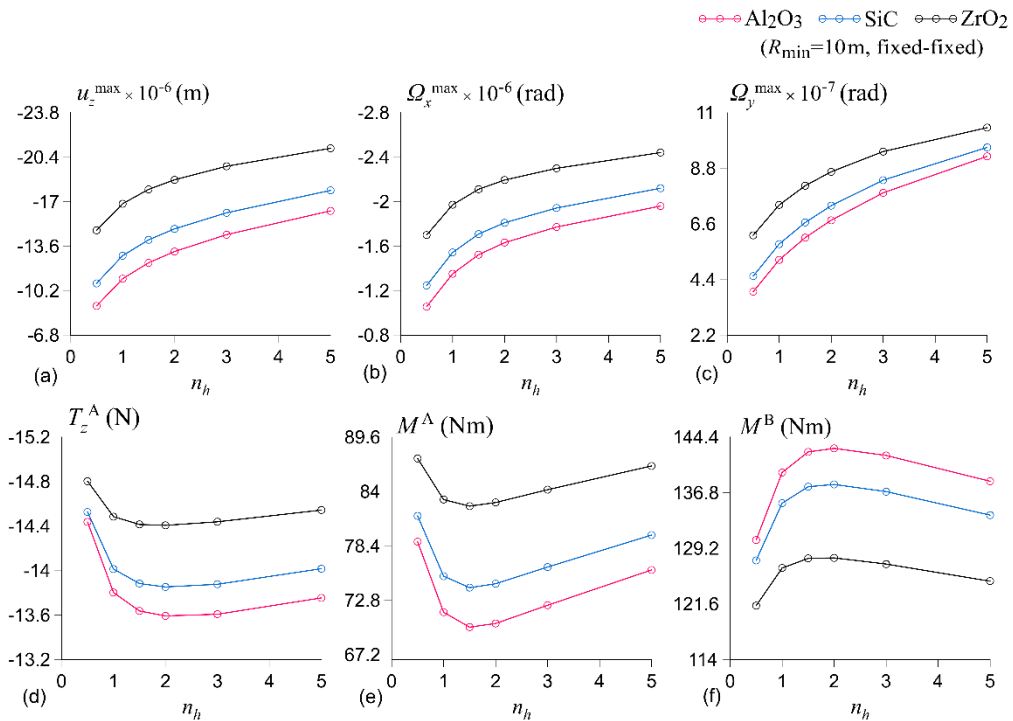

Fig. 8. The static responses of AFG circular beams ($R_{\max} = R_{\min} = 10$ m) having fixed-fixed BC

Table 5. The normalized arc length coordinates for the maximum displacement $u_z^{\max}$ of AFG planar curved beam with $R_{\max} = 10$ m for the fixed-fixed boundary condition.

| Minimum radius	Ceramic materials	The non-homogeneity index (n_h)					
		0.5	1	1.5	2	3	5
$R_{\min}$= 5 m	Al$_2$O$_3$	0.448	0.448	0.435	0.435	0.435	0.448
	SiC	0.474	0.448	0.448	0.448	0.448	0.461
	ZrO$_2$	0.474	0.461	0.461	0.461	0.461	0.474
$R_{\min}$= 7.5 m	Al$_2$O$_3$	0.455	0.443	0.432	0.432	0.432	0.443
	SiC	0.455	0.455	0.443	0.443	0.443	0.455
	ZrO$_2$	0.477	0.455	0.455	0.455	0.455	0.466
$R_{\min}$ = 10 m	Al$_2$O$_3$	0.460	0.440	0.440	0.440	0.440	0.440
	SiC	0.460	0.460	0.440	0.440	0.440	0.450
	ZrO$_2$	0.480	0.460	0.460	0.460	0.460	0.460
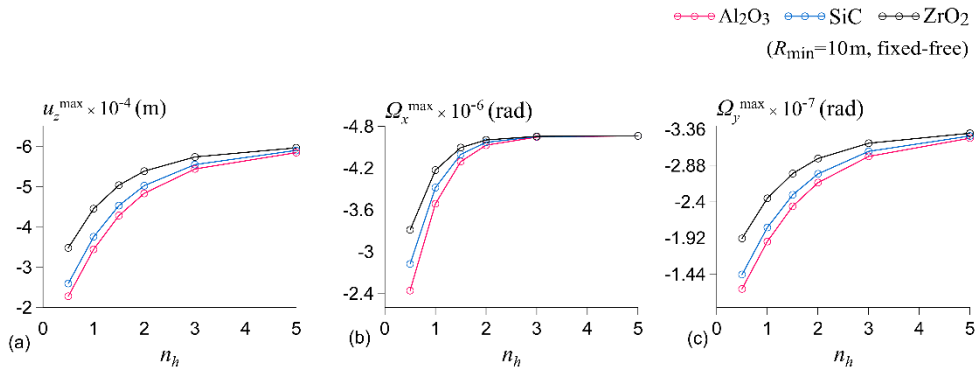
Fig. 9. The static responses of AFG circular beams ($R_{\max} = R_{\min} = 10$ m) having fixed-free BC

3.2.2.1. The effect of the non-homogeneity index (n_h)

To investigate the effect of the non-homogeneity index on the static responses of AFG elliptical beam, the results of the cases n_h = 1, 1.5, 2, 3, and 5 are compared with those of the case n_h = 0.5 using $\beta_{n_h=i}^{\Theta} = \Theta_{n_h=i} / \Theta_{n_h=0.5}$ where ($\Theta : u, T, M$ and i = 1, 1.5, 2, 3, or 5) for each boundary condition, minimum radius, and ceramic material.

For $u_z^{\max}$, the minimum and maximum ratios $\beta_{n_h=i}^{u_z^{\max}}$ are obtained as i = 1 and 5, respectively (Table 6). When the non-homogeneity index increases, the ratio $\beta_{n_h}^{u_z^{\max}}$ increases. The values $\beta_{n_h}^{u_z^{\max}}$ are greater than 1. Also, the ratio $\beta_{n_h}^{u_z^{\max}}$ of the fixed-free BC case is greater than that of the fixed-fixed BC case.

In the fixed-fixed case, the value of each ratio $\beta_{n_h=i}^{T_z^{A}}$, $\beta_{n_h=i}^{M^{A}}$ and $\beta_{n_h=i}^{M^{B}}$ remains approximately the same for each ceramic material and minimum radius. The average and standard deviations $\bar{\beta}_{n_h}^{T_z^{A}}$, $\bar{\beta}_{n_h}^{M^{A}}$ and $\bar{\beta}_{n_h}^{M^{B}}$ over the non-homogeneity index are calculated for the static responses $\beta_{n_h=i}^{T_z^{A}}$, $\beta_{n_h=i}^{M^{A}}$ and $\beta_{n_h=i}^{M^{B}}$ of the AFG elliptical planar beam, respectively. For each minimum radius and ceramic material, the values $\bar{\beta}_{n_h}$ are tabulated in Table 7.

Table 6. The ratio $\beta_{n_h}^{u_z^{max}}$ of AFG elliptical planar beam for fixed-fixed and fixed-free boundary conditions

Case	Ceramic materials	$R_{min} = 5$ m		$R_{min} = 7.5$ m		$R_{min} = 10$ m	
		$n_h = 1$	$n_h = 5$	$n_h = 1$	$n_h = 5$	$n_h = 1$	$n_h = 5$
fixed-fixed	Al$_2$O$_3$	1.264	2.149	1.245	1.941	1.229	1.804
	SiC	1.229	1.931	1.211	1.769	1.196	1.660
	ZrO$_2$	1.160	1.583	1.147	1.488	1.138	1.424
fixed-free	Al$_2$O$_3$	1.513	2.663	1.513	2.595	1.512	2.568
	SiC	1.441	2.315	1.444	2.281	1.446	2.273
	ZrO$_2$	1.285	1.748	1.282	1.723	1.280	1.714

Table 7. The average and standard deviation $\bar{\beta}_{n_h}$ for the static responses (T_z^A, M^A and M^B) of an AFG elliptical planar beam having fixed-fixed BC

Parameters	Ceramic materials	$R_{min} = 5$ m	$R_{min} = 7.5$ m	$R_{min} = 10$ m
T_z^A	Al$_2$O$_3$	0.958 ± 0.007	0.953 ± 0.006	0.947 ± 0.007
	SiC	0.967 ± 0.006	0.963 ± 0.005	0.959 ± 0.005
	ZrO$_2$	0.997 ± 0.010	0.979 ± 0.004	0.977 ± 0.004
M^A	Al$_2$O$_3$	0.934 ± 0.039	0.923 ± 0.033	0.914 ± 0.030
	SiC	0.950 ± 0.035	0.940 ± 0.029	0.932 ± 0.027
	ZrO$_2$	1.003 ± 0.029	0.965 ± 0.021	0.960 ± 0.019
M^B	Al$_2$O$_3$	1.111 ± 0.021	1.091 ± 0.015	1.082 ± 0.015
	SiC	1.092 ± 0.017	1.076 ± 0.013	1.069 ± 0.014
	ZrO$_2$	1.011 ± 0.023	1.050 ± 0.010	1.045 ± 0.011

   To investigate the effect of the non-homogeneity index and ceramic inclusions on the resultant moments of support reactions at points A and B (Fig.1), the ratio M^A / M^B is calculated for each minimum radii as follows: The maximum M^A / M^B occurs at ceramic-rich material case ($n_h = 0.5$) for all considered ceramic inclusions and minimum radii. For $R_{min} = 5$ m, it is calculated as 0.750, 0.676, and 0.648 for ZrO$_2$, SiC and Al$_2$O$_3$, respectively. For $R_{min} = 7.5$ m, we have the values of 0.736, 0.658, and 0.627 for ZrO$_2$, SiC, and Al$_2$O$_3$, respectively. For $R_{min} = 10$ m, the results become 0.720, 0.639, and 0.605 for ZrO$_2$, SiC, and Al$_2$O$_3$, respectively.

   The minimum M^A / M^B for all considered ceramic inclusions and minimum radii occurs at $n_h = 1.5$ except $R_{min} = 5$ m and Al$_2$O$_3$ case ($n_h = 2.0$). For $R_{min} = 5$ m, the minimum ratios of ZrO$_2$, SiC and Al$_2$O$_3$ cases are 0.672, 0.568, and 0.525, respectively. For $R_{min} = 7.5$ m, these are 0.661, 0.556 and 0.511, respectively. For $R_{min} = 10$ m, they are 0.645, 0.538 and 0.492, respectively.

3.2.2.2. The effect of the material properties of ceramic material

To investigate the effect of the ceramic material on the static responses of the AFG elliptical beam, the results of the cases SiC and ZrO$_2$ are compared with those of Al$_2$O$_3$ using $\beta_c^{\Theta} = \Theta_c / \Theta_{Al_2O_3}$ where ($\Theta : u, T, M$, and c: SiC and ZrO$_2$) for each boundary condition, minimum radius, and the non-homogeneity index.

Table 8. The ratio $\beta_c^{u_z^{max}}$ of AFG elliptical planar beam for fixed-fixed and fixed-free boundary conditions

Case	Ceramic materials	$R_{min} = 5$ m		$R_{min} = 7.5$ m		$R_{min} = 10$ m	
		$n_h = 0.5$	$n_h = 5$	$n_h = 0.5$	$n_h = 5$	$n_h = 0.5$,	$n_h = 5$
fixed-fixed	SiC	1.197	1.075	1.192	1.086	1.191	1.096
	ZrO_2	1.672	1.232	1.648	1.264	1.639	1.293
fixed-free	SiC	1.159	1.007	1.147	1.008	1.140	1.009
	ZrO_2	1.548	1.016	1.533	1.018	1.528	1.020

Table 9. The average and standard deviation $\bar{\beta}_c$ for the static responses (T_z^A, M^A and M^B) of an AFG elliptical planar beam having fixed-fixed BC

Parameters	Ceramic materials	$R_{min} = 5$ m	$R_{min} = 7.5$ m	$R_{min} = 10$ m
T_z^A	SiC	1.013 ± 0.004	1.014 ± 0.005	1.016 ± 0.005
	ZrO_2	1.043 ± 0.011	1.047 ± 0.012	1.052 ± 0.014
M^A	SiC	1.042 ± 0.009	1.046 ± 0.009	1.051 ± 0.009
	ZrO_2	1.132 ± 0.025	1.142 ± 0.025	1.155 ± 0.026
M^B	SiC	0.971 ± 0.008	0.970 ± 0.006	0.969 ± 0.005
	ZrO_2	0.908 ± 0.019	0.907 ± 0.015	0.905 ± 0.014

For $\beta_c^{u_z^{max}}$, the maximum and minimum ratios $\beta_c^{u_z^{max}}$ are obtained for $n_h = 0.5$ and 5, respectively (Table 8). When the non-homogeneity index increases, the ratio $\beta_c^{u_z^{max}}$ decreases. The values $\beta_c^{u_z^{max}}$ are greater than 1. The ratio $\beta_c^{u_z^{max}}$ of the fixed-free BC is less than that of the fixed-fixed BC, and the ratio $\beta_c^{u_z^{max}}$ of the ZrO_2 case is greater than that of the SiC case.

In the case of fixed-fixed BC for the $n_h = 0.5, 1, 1.5, 2, 3$ and 5 values of the non-homogeneity index, the values $\beta_c^{T_z^A}$, $\beta_c^{M^A}$ and $\beta_c^{M^B}$ remains approximately the same for each ceramic material (c: SiC and ZrO_2) and minimum radius. The average and standard deviation $\bar{\beta}_c^{T_z^A}$, $\bar{\beta}_c^{M^A}$ and $\bar{\beta}_c^{M^B}$ over the non-homogeneity index are calculated for the static responses $\beta_c^{T_z^A}$, $\beta_c^{M^A}$ of the AFG elliptical planar beam, respectively. For each minimum radius and ceramic material (SiC and ZrO_2), the values $\bar{\beta}_c$ are tabulated in Table 9.

4. Conclusions

The static and free vibration responses of axially functionally graded elliptical beams are investigated using a mixed finite element method. Functionally graded material is composed of metal-matrix (Al) and ceramic inclusions (Al_2O_3, SiC, and ZrO_2). The effect of the non-homogeneity index, ceramic-particle material, minimum radius, and boundary conditions on the static and dynamic response of the AFG elliptical beam is discussed in detail (Sec. 3.2). The main outcomes of the parametric analysis can be summarized as follows:
a) Free vibration analysis (Sec.3.2.1):
- As the minimum radius R_{min} increase, the fundamental natural frequencies decrease for all the considered ceramic particles, the non-homogeneity indices, and boundary conditions cases.
- When the effect of ceramic particle materials is considered for all the considered non-homogeneity indexes, minimum radii, and boundary conditions, the maximum fundamental natural frequencies of the

fixed-fixed boundary condition are obtained for the Al_2O_3 case whereas the maximum natural frequencies of the fixed-free boundary condition are obtained for the SiC. The minimum fundamental natural frequencies are obtained for ZrO_2 for both boundary conditions.

- When the non-homogeneity index n_h increase, the fundamental natural frequencies of the fixed-free beam increase for all the considered ceramic-particle and minimum radii cases.
- In cases Al_2O_3 and SiC, since the constituent of the fixed-fixed AFG beam becomes metal-rich ($n_h \uparrow$), the fundamental natural frequencies decrease, and more ductile behavior can be obtained. However, in the case of ZrO_2, it is quite the opposite.
- As the ratio R_{min} / R_{max} decreases, the change of non-homogeneity index is more influential on the results of fundamental natural frequencies of Al_2O_3 and SiC cases whereas the change of non-homogeneity index is less influential on the results of fundamental natural frequencies of ZrO_2 case.

b) Static analysis (Sec.3.2.2):

- As the non-homogeneity index (n_h) increases, the constituent of functionally graded material along the beam axis becomes metal-rich material. Each ceramic-inclusions Al_2O_3, SiC and ZrO_2 has both higher elasticity modulus than that of the metal matrix (Al). Thus, the absolute value of static responses u_z^{max}, Ω_x^{max} and Ω_y^{max} increases for both fixed-fixed and fixed-free boundary conditions, respectively.
- In the case of the fixed-fixed boundary condition, the absolute maximum and minimum values of u_z^{max}, Ω_x^{max}, Ω_y^{max} are obtained for the ceramic materials Al_2O_3 and ZrO_2, respectively. When the non-homogeneity index increases, the change in the absolute values of T_z^A, M^A, and M^B has an opposite trend. Also, by considering the support reactions of points A and B, the maximum resultant moments M of the AFG beam occurs at point A for all considered non-homogeneity indices, the minimum radii, and ceramic inclusions.
- In the case of the fixed-free boundary condition, as the constituent of the AFG beam becomes metal-rich ($n_h \uparrow$), the effect of different ceramic materials on the static responses u_z^{max}, Ω_x^{max}, Ω_y^{max} quickly decreases. Each static response u_z^{max}, Ω_x^{max}, Ω_y^{max} approaches the same values for each ceramic material Al_2O_3, ZrO_2, and SiC by increasing the non-homogeneity index(n_h).

As far as the knowledge of the authors, the static and free vibration analysis of axially FG elliptical beam using mixed FEM is an original example for the literature.

Declaration of conflicting interests

The author(s) declared no potential conflicts of interest with respect to the research, authorship, and/or publication of this article.

References

[1] Chin ESC (1999) Army focused research team on functionally graded armor composites. Mater Sci Eng A 259:155–161. https://doi.org/10.1016/S0921-5093(98)00883-1
[2] Pompe W, Worch H, Epple M, et al (2003) Functionally graded materials for biomedical applications. Mater Sci Eng A 362:40–60. https://doi.org/10.1016/S0921-5093(03)00580-X
[3] Miyamoto Y, Kaysser WA, Rabin BH, Kawasaki A, Ford RG (2013) Functionally Graded Materials: Design, Processing, and Applications (Vol. 5). Springer Science & Business Media.
[4] Kumar S, Reddy KVVSM, Kumar A, Devi GR (2013) Development and characterization of polymer–ceramic continuous fiber-reinforced functionally graded composites for aerospace application. Aerosp Sci Technol 26:185–191. https://doi.org/10.1016/j.ast.2012.04.002

[5]   Zhang C, Chen F, Huang Z, et al (2019) Additive manufacturing of functionally graded materials: A review. Mater Sci Eng A 764:138209. https://doi.org/10.1016/j.msea.2019.138209

[6]   Sofiyev AH (2019) Review of research on the vibration and buckling of the FGM conical shells. Compos Struct 211:301–317. https://doi.org/10.1016/j.compstruct.2018.12.047

[7]   Adıyaman G, Birinci A (2018) A general solution for the receding contact problem of a functionally graded layer resting on a Winkler foundation. Journal of Structural Engineering & Applied Mechanics 1(3):136–146. https://doi.org/10.31462/jseam.2018.03136146

[8]   Haciyev VC, Mirzeyeva GR, Shiriyev AI (2018) Effect of Winkler foundation, inhomogeneity and orthotropy on the frequency of plates. Journal of Structural Engineering & Applied Mechanics 1(1):1–5. https://doi.org/10.31462/jseam.2018.01001005

[9]   Karakaş Aİ, Daloğlu A (2019) A parametric frequency analysis for functionally graded cylinders using graded harmonic FEM. Journal of Structural Engineering & Applied Mechanics 2(4):190–206. https://doi.org/10.31462/jseam.2019.04190206

[10] Polat A, Kaya Y, Bora P, Bendine K, Özşahin TŞ (2019) Investigation of the contact problem for a partial functionally graded layer by using finite element method. Journal of Structural Engineering & Applied Mechanics 1(4):185–193. https://doi.org/10.31462/jseam.2019.01185193

[11] Garg A, Belarbi M-O, Chalak HD, Chakrabarti A (2021) A review of the analysis of sandwich FGM structures. Compos Struct 258:113427. https://doi.org/10.1016/j.compstruct.2020.113427

[12] Piovan MT, Domini S, Ramirez JM (2012) In-plane and out-of-plane dynamics and buckling of functionally graded circular curved beams. Compos Struct 94:3194–3206. https://doi.org/10.1016/j.compstruct.2012.04.032

[13] Swaminathan K, Naveenkumar DT, Zenkour AM, Carrera E (2015) Stress, vibration and buckling analyses of FGM plates—A state-of-the-art review. Compos Struct 120:10–31. https://doi.org/10.1016/j.compstruct.2014.09.070

[14] Avey A, Süzer M (2019) The investigation of dynamic response of FGM cylindrical shells in mixed boundary conditions, Nigde Omer Halisdemir University Journal of Engineering Science. 8(3):1-15. https://doi.org/10.28948/ngumuh.617259. (in Turkish)

[15] Norris CH, Wilbur JB, Utku Ş (1977) Elementary Structural Analysis. McGraw-Hill.

[16] Prathap G (1985) The curved beam/deep arch/finite ring element revisited. Int J Numer Methods Eng 21(3):389-407. https://doi.org/10.1002/nme.1620210302.

[17] Chidamparam P, Leissa AW (1993) Vibrations of planar curved beams, rings, and arches. Appl Mech Rev 46:467–483. https://doi.org/10.1115/1.3120374

[18] Cazzani A, Malagù M, Turco E (2016) Isogeometric analysis of plane-curved beams. Math Mech Solids 21:562–577. https://doi.org/10.1177/1081286514531265

[19] Caliò I, Elishakoff I (2005) Closed-form solutions for axially graded beam-columns. J Sound Vib 280:1083–1094. https://doi.org/10.1016/j.jsv.2004.02.018

[20] Aydogdu M (2008) Semi-inverse method for vibration and buckling of axially functionally graded beams. J Reinf Plast Compos 27:683–691. https://doi.org/10.1177/0731684407081369

[21] Şimşek M, Kocatürk T, Akbaş ŞD (2012) Dynamic behavior of an axially functionally graded beam under action of a moving harmonic load. Compos Struct 94:2358–2364. https://doi.org/10.1016/j.compstruct.2012.03.020

[22] Babilio E (2013) Dynamics of an axially functionally graded beam under axial load. Eur Phys J Spec Top 222:1519–1539. https://doi.org/10.1140/epjst/e2013-01942-8

[23] Shafiei N, Kazemi M, Ghadiri M (2016) Nonlinear vibration of axially functionally graded tapered microbeams. Int J Eng Sci 102:12–26. https://doi.org/10.1016/j.ijengsci.2016.02.007

[24] Azimi M, Mirjavadi SS, Shafiei N, Hamouda AMS (2016) Thermo-mechanical vibration of rotating axially functionally graded nonlocal Timoshenko beam. Appl Phys A 123:104. https://doi.org/10.1007/s00339-016-0712-5

[25] Li X, Li L, Hu Y, et al (2017) Bending, buckling and vibration of axially functionally graded beams based on nonlocal strain gradient theory. Compos Struct 165:250–265. https://doi.org/10.1016/j.compstruct.2017.01.032

[26] Shafiei N, Kazemi M, Ghadiri M (2016) Nonlinear vibration of axially functionally graded tapered microbeams. Int J Eng Sci 102:12–26. https://doi.org/10.1016/j.ijengsci.2016.02.007

[27] Ghayesh MH (2018) Nonlinear vibration analysis of axially functionally graded shear-deformable tapered beams. Appl Math Model 59:583–596. https://doi.org/10.1016/j.apm.2018.02.017

[28] Singh A, Kumari P (2018) Analytical solution of functionally graded beam having longitudinal stiffness variation. Int J Comput Methods Eng Sci Mech 19:390–395. https://doi.org/10.1080/15502287.2018.1534152

[29] Zheng S, Chen D, Wang H (2019) Size-dependent nonlinear free vibration of axially functionally graded tapered microbeams using finite element method. Thin-Walled Struct 139:46–52. https://doi.org/10.1016/j.tws.2019.02.033

[30] Ermis M, Aribas UN, Kutlu A, Eratlı N, Omurtag MH (2019) Forced vibration analysis of axially FG straight beams by mixed FEM. IV. Eurasian Conference on Civil and Environmental Engineering, İstanbul, Türkiye, pp.894-899.

[31] Aribas UN, Ermis M Kutlu A, Eratlı N, Omurtag MH (2019) Elastically Damped Transient Response of Axially FG Straight Beams. International Journal of Theoretical and Applied Mechanics 4:19-25.

[32] Rajasekaran S (2014) Analysis of curved beams using a new differential transformation-based curved beam element. Meccanica 49:863–886. https://doi.org/10.1007/s11012-013-9835-3

[33] Tsiatas GC, Charalampakis AE (2017) Optimizing the natural frequencies of axially functionally graded beams and arches. Compos Struct 160:256–266. https://doi.org/10.1016/j.compstruct.2016.10.057

[34] Noori AR, Aslan TA, Temel B (2018) An efficient approach for in-plane free and forced vibrations of axially functionally graded parabolic arches with nonuniform cross-section. Compos Struct 200:701–710. https://doi.org/10.1016/j.compstruct.2018.05.077

[35] Temel B, Noori AR (2019) Out-of-plane vibrations of shear-deformable AFG cycloidal beams with variable cross-section. Appl Acoust 155:84–96. https://doi.org/10.1016/j.apacoust.2019.05.010

[36] Lee JK, Lee BK (2019) In-plane free vibration of uniform circular arches made of axially functionally graded materials. Int J Struct Stab Dyn 19:1950084. https://doi.org/10.1142/S0219455419500846

[37] Aribas UN, Ermis M, Omurtag MH (2021) The static and stress analyses of axially functionally graded exact super-elliptical beams via mixed FEM. Arch Appl Mech 91, 4783–4796. https://doi.org/10.1007/s00419-021-02033-w

[38] Aktı Z, Ermis M, Omurtag M.H (2021) Static analysis of axially functionally graded circular beams via mixed finite element method. TUMTMK 22nd National Mechanics Congress, Çukurova University-Adana, Turkey (in Turkish), 525-539. ISBN: 978-975-561-523-3.

[39] Kır O, Ermis M, Aribas UN, Omurtag MH (2021) Static analysis of axially functionally graded elliptical beams via finite element method. TUMTMK 22nd National Mechanics Congress, Çukurova University-Adana, Turkey (in Turkish), 46-60. ISBN: 978-975-561-523-3.

[40] Aydoğan G, Ermis M, Aribas UN, Omurtag M.H (2021) Free vibration analysis of axially functionally graded elliptical beams via finite element method. TUMTMK 22nd National Mechanics Congress, Çukurova University-Adana, Turkey (in Turkish), 61-74. ISBN: 978-975-561-523-3.

[41] Ermis M, Omurtag MH (2017). Static and dynamic analysis of conical helices based on exact geometry via mixed FEM. Int J Mech Sci 131-132:296-304. https://doi.org/10.1016/j.ijmecsci.2017.07.010

[42] Voigt W. (1889) Ueber die beziehung zwischen den beiden elasticitätsconstanten isotroper körper. Ann Phys. 274(12):573–87.

[43] Karami B, Shahsavari D, Janghorban M, Li L (2019) Influence of homogenization schemes on vibration of functionally graded curved microbeams. Compos Struct 216:67–79. https://doi.org/10.1016/j.compstruct.2019.02.089

[44] Fu T, Chen Z, Yu H, et al (2018) An analytical study of sound transmission through corrugated core FGM sandwich plates filled with porous material. Compos Part B Eng 151:161–172. https://doi.org/10.1016/j.compositesb.2018.06.010

[45] Gunes R, Aydin M, Apalak MK, Reddy JN (2014) Experimental and numerical investigations of low-velocity impact on functionally graded circular plates. Compos Part B Eng 59:21–32. https://doi.org/10.1016/j.compositesb.2013.11.022

[46] Omurtag MH, Aköz AY (1992) The mixed finite element solution of helical beams with variable cross-section under arbitrary loading. Comput Struct 43:325–331. https://doi.org/10.1016/0045-7949(92)90149-T

[47] Eratli N, Yilmaz M, Darilmaz K, Omurtag MH (2016) Dynamic analysis of helicoidal bars with non-circular cross-sections via mixed FEM, Struct Eng Mech 57:221–238. https://doi.org/10. 12989/sem.2016.57.2.221.

[48] Ermiş M (2021) Free vibration analysis of axially functionally graded helices via mixed finite element method. Nigde Omer Halisdemir University Journal of Engineering Science 10(1):319-327. https://doi.org/10.28948/ngmuh.823385 (in Turkish)

[49] Oden JT, Reddy JN (1976) An Introduction to the Mathematical Theory of Finite Elements. JohnWiley&Sons Inc., NewYork.

[50] Ansys® Academic Research Mechanical, Mechanical APDL Release 2021 R1, Element Reference, ANSYS, Inc.